**WSRC-TR-2003-00077
ITER/US/02/INV-VV-01**

WELDABILITY COMPARISON OF TRITIUM-CHARGED-AND-AGED 304 AND 316LN STAINLESS STEELS (U)

By:

M. H. Tosten
W. R. Kanne, Jr.
G. K. Chapman
S. L. West
B. J. Cross

May 2003

A report written in support of the International
Thermonuclear Experimental Reactor (ITER)
under Task Agreement G 15 TT 12 96-05-15 FU,
Subtask 5, Phase 1, Part 3.

Westinghouse Savannah River Company
Aiken, SC 29808

PREPARED FOR THE U.S. DEPARTMENT OF ENERGY
UNDER CONTRACT DE-AC09-96SR18500

Acknowledgement

"This report is an account of work assigned to the U.S. Home Team under Task Agreement No. G 15 TT 96-05-15 FU within the Agreement among the European Atomic Energy Community, the Government of Japan, the Government of the Russian Federation, and the Government of the United States of America on Cooperation in the Engineering Design Activities for the International Thermonuclear Experimental Reactor ("ITER EDA Agreement") under the auspices of the International Atomic Energy Agency (IAEA). The report has not been reviewed by the ITER Publications Office."

WSRC-TR-2003-00077
ITER/US/02/INV-VV-01

SMTD
SRATEGIC MATERIALS TECHNOLOGY DEPARTMENT

Keywords: Helium Embrittlement
Stainless Steel
Weld Cracks

Retention: Permanent

WELDABILITY COMPARISON OF TRITIUM-CHARGED-AND-AGED 304 AND 316LN STAINLESS STEELS (U)

By:

M. H. Tosten
W. R. Kanne, Jr.
G. K. Chapman
S. L. West
B. J. Cross

Issued: May 2003

SRTC SAVANNAH RIVER TECHNOLOGY CENTER, AIKEN, SC 29808
Westinghouse Savannah River Company
Prepared for the U.S. Department of Energy under Contract DE-AC09-96SR18500

WSRC-TR-2003-00077
ITER/US/02/INV-VV-01

WELDABILITY COMPARISON OF TRITIUM-CHARGED-AND-AGED 304 AND 316LN STAINLESS STEELS (U)

By:

M. H. Tosten
W. R. Kanne, Jr.
G. K. Chapman
S. L. West
B. J. Cross

Westinghouse Savannah River Company
Savannah River Technology Center
Aiken, SC 29808

ABSTRACT

Measurement of the effects of helium (from tritium decay) on the weldability of Types 304 and ITER Grade 316LN stainless steel demonstrated the inherent complexities in designing and conducting an experimental program using tritium-charged-and-aged materials to simulate the effects of irradiation-induced helium on weld behavior. Differences in microstructure, surface condition and alloy chemistry are known to play key roles in tritium absorption and distribution and thus have direct effects on the subsequent ^{3}He production and distribution. The helium embrittlement cracking produced in 0.5 in. (12.7 mm) thick 304 and 316LN plates that were tritium-charged in the same container and subsequently welded with gas metal arc, low heat input weld overlays and gas tungsten arc stringer beads, varied markedly. For example, the porosity in the weld beads was much higher in the 304 plate than in the 316LN plate. Additionally, crack measurements from weld cross-sections revealed more extensive intergranular cracking in the heat-affected zones of welds on the 304 plate when compared to the 316LN plate. However, the differences between the two types of stainless steel may not be a result of differences in the resistance to helium embrittlement cracking, but may be due to initial tritium concentration differences developed in the as-charged plates. Further work is necessary to identify the reasons for the apparent plate to plate variation in tritium/helium content and to demonstrate the similarities (or differences) between Types 304 and ITER grade 316LN stainless steel.

TABLE OF CONTENTS

	Page No.
ABSTRACT	1
TABLE OF CONTENTS	2
TASK SPECIFICATIONS	3
INTRODUCTION	3
EXPERIMENTAL PROCEDURE	4
RESULTS	6
Helium Analysis	6
Metallographic Examination	6
TEM Examination	7
Crack and Porosity Measurements	8
DISCUSSION	9
CONCLUSIONS	10
FUTURE PLANS	11
ACKNOWLEDGEMENTS	11
REFERENCES	12
TABLES	
1. Alloy Composition	14
2. Tritium-Charging Schedule	14
3. Welding Conditions	15
4. Crack Analysis Summary - GMA Overlay Welds	17
5. Crack Analysis Summary - GTA Stringer Beads	18
FIGURES	
1. Typical Weld/Plate Configuration	19
2. Schematic Diagram Illustrating Heat Input Variables	20
3. Toe Cracking in HAZ of Stringer Bead on 304 Plate	21
4. Cracking Beneath an Overlay Weld on the 304 Plate	22
5. Cross-Sections of Stringer Beads in 304 and 316LN	23
6. TEM Image of He Bubbles in 316LN - Slice 1	24
7. TEM Image of He Bubbles in 316LN - Slice 2	25
8. Total Crack Length for Overlays and Stringer Beads	26
9. Normalized Crack Length vs. Heat Input - Stringer Beads	26
10. Total crack Length vs. Heat Input - Stringer Beads	27
11. Porosity vs. Heat Input - Stringer Beads 304 and 316LN	27
12. Total Crack Length vs. Helium Concentration	28

TASK SPECIFICATIONS

This report is in fulfillment of task Agreement G 15 TT 12 96-05-15 FU (Vacuum Vessel Section Models, Blanket Support Structures, and Welding, Cutting, and Inspection Development for the VV and Blanket (T204-9)); Subtask 5 (Welding Comparison of Irradiated and Tritium Charged SS); Phase 1 (Sample Preparation and Testing); Part 3 (Weldability of Helium Charged 316 vs. 304 SS)

Work Specifications: Tritium-charged-and-aged 304 and 316LN-IG stainless steel plates will be used as substrate materials for GMA (MIG) overlay welds and a series of autogenous GTA stringer beads. Metallographic examinations will be conducted on the plates to characterize the embrittlement that occurred during welding. A direct comparison of these two materials will help validate the large data set on the weldability of 304 stainless steel to the ITER material of construction.

INTRODUCTION

This work is part of the program to develop methods for repair or replacement of components in the next step fusion devices, such as a thermonuclear experimental reactor. The current weldability study is the final part of a three-part program funded at the Savannah River Technology Center (SRTC). The first two parts, previously completed, were 1) the development of a model for helium embrittlement [Ref. 1], and 2) a transmission electron microscopy (TEM) investigation of overlay welds made on irradiated 304 stainless steel [Ref. 2]. The final part of the program is a comparison of helium embrittlement cracking caused by welding 304 stainless steel and 316LN stainless steel containing helium from tritium decay and is the subject of this report.

Work at the Savannah River Site (SRS) has shown that conventional welding processes on stainless steels are strongly affected by the presence of helium. This was evidenced initially in attempts to repair an irradiated reactor tank wall [Ref. 3,4]. Helium embrittlement cracking was observed in the weld heat-affected zones (HAZs) in the "repaired" areas. Subsequent research led to the development of a low heat input gas metal arc (GMA) welding technique suitable for welding on stainless steels, both irradiated and tritium-charged-and-aged, with a minimum of underbead and toe cracking up to helium levels of 220 appm [Ref. 5]. This technique employs an oscillating torch to produce a cladding of filler metal approximately 0.035 in. (0.9 mm) thick with a depth of penetration into the base metal of only 0.003 in. (0.08 mm).

Weldability with the overlay technique was compared at SRS with conventional gas tungsten arc (GTA) and GMA welding techniques. The welding methods were also compared for irradiated vs. tritium charged-and-aged 304 stainless steel [Ref. 6]. Results showed the overlay technique to be a significant improvement over conventional welding methods. Surface toe cracking was eliminated with the overlay technique. Cracking, both toe and underbead, was much less in the tritium-charged-and-aged stainless steel than in the irradiated 304 stainless steel for a given helium concentration.

One material of choice for a next step fusion device is Type 316LN stainless steel. Limited data is available on the weldability of thick sections of this material in the presence of entrapped helium from either exposure to 1) neutron fluences and the generation of ^{4}He or 2) high-pressure tritium gas and the subsequent decay to ^{3}He.

Investigations of the weldability of thin sections of 316 stainless steel doped with helium have been carried out at the Oak Ridge National Laboratory in cooperation with Auburn University [Ref. 7,8]. These investigations have shown that 316 stainless steel responds in a qualitatively similar way to 304L stainless steel when welded after helium impregnation. That is, both are embrittled by the helium and the embrittlement is intergranular due to the growth of helium bubbles on the grain boundaries. The weldability investigations at ORNL/Auburn were carried out on very thin (0.030 in.) material. Compressive applied stress was shown to reduce or eliminate cracking in these thin sections. A threshold of 1 appm helium was suggested below which cracking would not occur for repair welds in irradiated 316 stainless steel.

The weldability of irradiated 304 and 316 stainless steels has also been investigated in other countries, particularly Japan, but a direct comparison between the two materials has not been made. Results support the findings that heat input is important to reduce cracking [Ref. 9], that mechanical properties are affected by the helium embrittlement cracking [Ref. 10], and that the amount of cracking is proportional to the helium content.

The ^{3}He/helium bubble distribution that forms in tritium-charged-and-aged stainless steels is dependent upon the tritium concentration profile that exists in the material prior to and during aging as well as the microstructure of the material. Louthan et al. [Ref. 11] have shown that surface condition and microstructure strongly influence tritium adsorption in Type 304L stainless steel. Tritium uptake is expected to be complicated further by alloying additions (including nitrogen) as is hydrogen in austenitic stainless steels [Ref. 12,13]. The work of Morgan et al. [Ref.14] on tritium-charged-and-aged austenitic stainless steels shows that once tritium is present, the helium bubble distribution that develops during aging is determined by the base microstructure of these alloys and that this distribution has a considerable effect on fracture toughness and deformation mode. Additionally, the helium bubble microstructure that forms in weld HAZs [Ref 15,16] develops as a result of starting microstructure, weld conditions and plastic strain caused by weld shrinkage stresses.

In the current comparison study, a series of nine (9) 316LN and 304 stainless steel test plates were exposed to high-pressure tritium and aged to produce ^{3}He. GMA overlays were applied to the plates along with a series of GTA stringer beads to accentuate embrittlement effects. Due to funding limitations, only one plate from each alloy was examined in detail. A detailed comparison of the helium embrittlement cracking exhibited by both materials was conducted. The results of this study illustrate some of the difficulties in designing a comparative weldability study using tritium-charged-and-aged materials.

EXPERIMENTAL PROCEDURE

Materials for this study were obtained from a special, high-carbon lot of Type 304 used in a previous welding study at the SRTC [Ref. 5] and a special grade of 316LN (316LN-IG)

proposed for use in the fabrication of fusion reactor components. The starting materials were received in the solution annealed and quenched condition. The alloy chemistries are shown in Table 1. The two (2) plates examined in this study were part of a group of nine (9) plates that were electrical discharge machined from the as-received materials to serve as a weld substrate matrix. These plates varied in thickness from 0.030 in. (0.8 mm) to 0.5 in. (12.7 mm) and measured 4.07 in. (103.4 mm) in length by 1.25 in. (31.8 mm) in width. One test plate was cold-rolled by 50% to a thickness of 0.125 in. to provide a weld substrate with increased dislocation density to be compared with those from the as-received, solution annealed material. Also machined were eight (8) 0.030 in. thick test coupons to be used for helium analysis. All plates were ground with silicon carbide papers to remove any surface "damage" resulting from the machining operation. A "600 grit" surface finish was attained on all plates prior to tritium charging.

The nine (9) test plates were divided into two (2) groups for tritium charging (see Table 2). Each group was charged separately due to limited space in the pressure vessel. Samples were held at 350°C for two (2) weeks at a tritium overpressure of approximately 5000 psi. Tritium diffusion calculations (based on 304 data) showed that charging conditions were sufficient to completely saturate all but the 0.5 in. specimens with tritium. As a result, a tritium/helium concentration gradient was expected to exist in each of the 0.5 in. plates. The two (2) plates analyzed in the current study were charged in the first charging run (Run #1).

Upon completion of each run, the charging vessel was cooled to room temperature and depressurized. All specimens were subsequently moved to a freezer and stored at -23°C to minimize tritium loss and to allow for helium ingrowth. Following aging (Run #1 - 9 months, Run #2 - 6 months), all samples were vacuum outgassed for three (3) weeks at 450°C to remove as much of the residual tritium as possible. Small pieces from the 0.030 in. thick test coupons were sent to Pacific Northwest National Laboratory (PNNL) for helium analysis.

All welding was performed in a fume hood designed for tritium use. Two different type welds were used in this study - GMA low heat input, oscillating, overlay welds and autogenous, GTA stringer beads. All welds were made with a shielding gas having a composition of 92% He, 7.5% Ar, 0.5% CO_2 at a rate 40 cfh. Plates were clamped to a heat sink to provide adequate heat transfer and restraint during welding. Overlay welds were made with 308L and 316L filler wire on the 304 and 316LN plates, respectively. Overlays were made on all plates except the 0.030 in. plate, which was too thin to provide a satisfactory weld substrate. Filler wires measured 0.035 in. (0.9 mm) in diameter except that used for the overlay on the 0.060 in. (1.5 mm) thick plate. A 0.023 in. (0.6 mm) diameter wire was used in that case to help reduce the heat damage to the plate.

GTA stringer beads were applied to plates using a variety of conditions in an attempt to 'bracket" any helium embrittlement effects. The conditions used for these welds, as well as those employed for the overlays, are listed in Table 3. Figure 1 is an image showing the series of welds made on a 0.5 in. thick 316LN plate. The tritium/helium-containing plate was placed between two uncharged plates that were used to begin (run-on tab) and end (run-off tab) the welds. Similar plate and weld configurations were used for the other test plates. Weld heat inputs were calculated using the parameters illustrated in Figure 2. This method allowed for direct comparison of the overlays to the stringer beads.

The two (2) 0.5 in. plates used for the present study were examined metallographically. Samples were first cleaned with a solution of Alconox® and water to remove welding residue. Visual inspections were conducted using a stereo microscope at 40X magnification to determine the extent of toe cracking in the weld HAZs.

Metallographic cross-sections were prepared from each weld using standard specimen preparation methods. All specimens were etched using a solution of 10% oxalic acid and water at 6 Vdc to reveal microstructural features and helium embrittlement (underbead) cracking. A montage of overlapping micrographs, taken at 50X magnification, was constructed for each weld cross-section. Cracks and weld porosity were measured and counted using these micrographs. Additional metallographic cross-sections were prepared from the tritiated and non-tritiated 304 plate according to ASTM Standard A262 in order to verify that the outgassing treatment (450°C for 3 weeks) did not cause sensitization in the tritiated plate.

TEM samples were prepared from beneath the GMA overlays on both plates. Thin slices were cut from the HAZs of both welds in an orientation parallel to the weld interface. Slices 1 and 2 were centered at approximately 0.010 in. (0.25 mm) and 0.050 in. (1.27 mm) from the weld interface, respectively. Control samples were sectioned in a similar manner, but from a region of each plate far removed from any welds. Disk specimens, measuring 3 mm in diameter, were punched from the slices and ground to a thickness of about 0.004 in. (0.1 mm). Specimens were polished to perforation with a twin jet electropolisher using a solution of 4 vol.% perchloric acid, 37 vol.% butylcellosolve, and 59 vol.% methanol. Polishing was accomplished using an applied potential of 35Vdc with the solution cooled to approximately -30°C. All specimens were examined in a JEOL 2010 operating at 200 kV.

RESULTS

Helium Analysis

The concentrations of helium in the 0.030 in. test coupons, determined by helium mass spectrometry at PNNL, were as follows: Run #1 - 85.6 appm (304), 91.3 appm (316LN) and Run #2 - 68.1 (304) and 65.7 (316LN). The reproducibility between duplicate analyses for each specimen averaged about 1%. The two (2) 0.5 in. plates used in this study were from Run #1 - the highest helium level. These 0.5 in. plates were not analyzed for helium content since test coupons from each alloy were believed to accurately represent the helium concentrations for all plates in each run.

Metallographic Examination

Analysis of the 0.5 in. plates at 40X magnification revealed no conclusive evidence of toe cracking in the HAZs of the GMA overlay welds in either the 304 or 316LN material. However, extensive toe cracking was observed in the HAZs of the GTA stringer beads. Figure 3 shows an example of toe cracking in the 304 plate. These cracks were observed in the HAZ of the weld made using the highest heat parameters. Cracks, like those shown, were visible along the entire length of this weld in the helium-containing plate. In general, cracking was much more pronounced in the 304 plate than in the 316LN, with the amount of

cracking in both plates increasing with weld heat input. Toe cracks were not observed in the HAZs of welds on the run-on or run-off tabs of either 0.5 in. test plate.

Microscopic examination of the polished and etched weld cross-sections showed numerous intergranular cracks in the HAZ of the overlay on the 304 plate (see Figure 4). Generally, cracks extended into the base metal by only a few grains. Infrequently, cracks also extended into the weld metal as evidenced in Figure 4. This observation demonstrates that cracking took place after solidification of the weld pool and not during weld production. Some cracking was observed beneath the overlay on the 316LN plate but to a much lesser degree when compared to the 304 material.

In contrast, cross-sections made from the GTA stringer beads revealed extensive intragranular cracking. Similar to the toe cracking, underbead cracking was much more pronounced in the HAZs of the GTA welds on the 304 plate when compared to the similar welds on the 316LN plate. These differences are illustrated in Figure 5. Welds shown in this figure were made using identical weld parameters. As can be seen, much more cracking occurred in the HAZ of the 304 weld (Figure 5a). Additionally, cracks extend into the 304 base material to a greater extent than the 316LN but crack lengths were still on the order of a few grains in length. It should be noted that underbead cracking was not observed in the HAZs of weld (overlays and stringer beads) cross-sections located on the run-on or run-off tabs of both plates.

Metallographic examination of the stringer beads also revealed more weld porosity in the 304 stringer beads when compared to like-welds in the 316LN plate (see Figure 5). This result is significant since weld porosity in helium-containing materials is directly related to helium content in the substrate material. Helium analyses from PNNL on test coupons from Run #1 yielded nearly identical results - 85.6 appm (304), 91.3 appm (316LN). The images in Figure 5 suggest that the results from the test coupons may not accurately represent the helium contents in the 0.5 in. plates.

TEM Examination

Control samples from the 316LN and 304 plates, centered at about 0.010 in. (0.25 mm, Slice 1) and 0.050 in. (1.27 mm, Slice 2) from the surface, consisted of equi-axed grains containing a low number density of dislocations and dislocation loops/stacking fault segments. Careful examination of the microstructure of both materials did not reveal any well-defined helium bubbles in the matrix or on the grain boundaries in this material. Contrast differences resembling bubbles were noted at some dislocations but these were too indistinct to be identified as bubbles. Small (<15 nm dia.), dislocation loops/stacking fault segments were more prevalent in the matrix of the 304 samples. These were shown previously to form as a result of helium bubble nucleation in the matrix [Ref. 15]. No actual bubbles were observed in association with these microstructural features in these materials.

Examination of TEM specimens sectioned from approximately 0.050 in. (Slice 2) beneath the 316LN overlay revealed an increase in dislocation density when compared to the control samples. Additionally, the presence of small (1-3 nm) helium bubbles was observed on some grain boundaries. Similar to the control sample, no obvious bubbles were observed in the grain interiors. Figure 6 is an image of a triple junction showing a large number of bubbles

associated with the grain boundaries. Figure 7 is an image from Slice 1. This image shows that the dislocation density has increased and that large helium bubbles have formed on the grain boundaries and within the matrix. The increase in dislocation density is caused by weld shrinkage stresses in the HAZ [Ref. 15]. The large bubbles form due to localized heating during the welding and the diffusion of helium, tritium and vacancies to the grain boundary and matrix bubbles. Plastic deformation in the HAZ also assists bubble growth via vacancy creation and dislocation/bubble interactions [Ref. 2].

Unfortunately, attempts to prepare thin foils from beneath the overlay weld on the 304 plate were unsuccessful. Severe cracking in the HAZ of the Slice 1 foils resulted in preferential but incomplete thinning in these areas. Additionally, Slice 2 foils appeared to thin only in regions of α'martensite revealing little of the base microstructure or helium bubble distribution. Although a thorough comparison was not possible, the microstructures (dislocation substructure and helium bubble distribution) that developed in the 316LN were consistent with those observed in a previous study [Ref. 15] of overlays on tritiated 304 substrate material.

Crack and Porosity Measurements

Crack analysis for both the overlays and the stringer beads was conducted by measuring the total number and length of cracks visible in each metallographic cross-section. To facilitate comparison, these measurements were normalized for differences in interface length. These data are summarized in Tables 4 and 5 and are shown graphically in Figures 8 - 10. Data in each of these figures are also represented as a least squares fit forced to a straight line. Figure 8 shows the comparison of total crack length for each heat input (denoted as the average heat input for each weld condition) for the overlays and stringer beads. Data for the stringer beads are further illustrated in Figures 9 and 10 which show the number of cracks per unit length of interface and the total crack length per unit length of interface versus heat input, respectively.

Measurements taken from beneath the GMA overlays show that there is about 12 times more cracking associated with the overlay on the 304 plate than with the overlay on the 316LN plate (Table 4). From Figure 8, it can be seen also that the total crack length per unit length of interface was about 33 times greater for the 304 when compared to the 316LN. A similar trend also exits for the GTA stringer beads. Crack totals for these welds were about 2 to 4 times greater in the HAZs on the 304 plate when compared to like welds (similar welding conditions) on the 316LN plate (Figure 9). Also, Figure 10 shows that the normalized crack lengths were 3-6 times greater for the welds on the 304 plate. The comparisons above are valid only if similar helium levels existed in 0.5 in. plates.

Micrographs of the weld cross-sections from both the overlays and stringer beads showed the presence of porosity in the welds (e.g., Figure 5). Porosity was measured as the number of gas bubbles greater than 20 μm in diameter. (Porosity smaller < 20 μm was too difficult to discern from other microstructural features.) Figure 11 is a plot of weld porosity versus weld heat input for the stringer beads. It is evident from this figure that the amount of porosity, at any given heat input, was greater in the welds on the 304 plate than in the welds on the 316LN plate. Furthermore, these data show that the number of gas bubbles increased with

heat input. These findings are believed to have a significant impact on the results of this study since the amount of weld porosity is an indication of helium content in the material.

DISCUSSION

The data illustrated in Figures 8, 9, 10 and 12 seem to illustrate that 316LN is less susceptible to cracking than the 304 material. However, Figure 11 (also see images in Figure 5) shows that the 304 stringer beads contained significantly more porosity than the 316 LN welds made using identical welding parameters. Porosity in welds on tritiated plates is associated with the evolution of helium from the base metal during the welding operation. The results shown in Figure 11 suggest that the helium concentration in the 304 plate is significantly greater than in the 316LN plate. This observation is at odds with the helium analyses performed at PNNL on unwelded coupons which showed that the helium concentrations of both steels were nearly the same: 85.6 appm - 304 and 91.3 appm - 316LN.

Samples submitted for helium analysis did not originate from the 0.5 in. plate but were instead taken from 0.030 in. thick plates specifically included in the charging runs for use as helium analysis coupons. These thin plates reached equilibrium while charging and the helium concentrations attained were believed to accurately represent the helium content in all of the plates up to 0.125 in. thickness as well as the surface regions of the 0.5 in. plates included in the charging runs. However, it is apparent from the porosity measurements (from metallographic cross-sections) that more helium is present in the 304 plate than the 316LN plate - at least at the depths affected by the weld beads.

The reasons for the presence of more helium in the 304 plate may be related to differences in microstructure, surface condition, and/or alloy chemistry. Louthan et al. [Ref. 11] have shown that the surface condition and the microstructure of 304L stainless steel can greatly affect tritium uptake. Surface barriers (oxide films) significantly limited tritium absorption in 304L stainless steel at tritium overpressures to 69MPa (10,000 psi). These authors also showed that, in addition to a grain size effect on tritium diffusion, increased cold work (higher dislocation density and more strain-induced martensite) enhanced the effective diffusivity of tritium in 304L. Even though great care was taken to ensure that the surface condition of all plates in the present study were the same (i.e., 600 grit finish), it is conceivable that differences may have existed that allowed for greater tritium uptake in the 304 plate. Additionally, microstructural variations between the two (2) plates including grain size, dislocation density, and the presence of martensitic phases may have resulted in increased tritium being present in the 304 plate after charging and subsequently more helium after aging.

Tritium uptake via high-pressure charging is expected to be complicated further by the presence of alloying elements. Sisson et al. [Ref. 12] have shown that the solubility of hydrogen in Type 21-6-9 stainless steel is approximately 40% higher than that of 304L. Like 316LN, nitrogen is added to 21-6-9 as a strengthening alloying element. These authors postulated that hydrogen segregates into the tensile strain field that exists around single nitrogen atoms or clusters of nitrogen atoms thus increasing hydrogen solubility. Similar behavior is anticipated for tritium. This result is contrary to observations in current study but it further illustrates the complexity of charging austenitic stainless steels with tritium.

S. Ningsen et al. [Ref. 13] also report that nitrogen increases hydrogen solubility in austenitic stainless steel. Additionally, these authors found that solubility is also related to the Cr and Ni content. High Cr and low Ni favors increased hydrogen solubility.

Work at SRS [Ref. 14] has shown that the helium distribution in tritium-charged-and-aged plates is influenced strongly by microstructure. In turn, the resulting helium bubble distribution greatly effects the embrittlement of stainless steels as well as observed failure modes. Austenitic steels (Types 304L, 316L and 21-6-9) containing helium exhibit reduced resistance to crack growth as well as a tendency toward intragranular fracture. Helium bubbles within the grain interiors and on grain boundaries enhance embrittlement by reducing the density of free dislocations, trapping hydrogen at grain boundaries and making deformation twinning and crack nucleation easier. The cracking observed in the HAZs of welds is strongly related to the initial tritium concentration profile and the helium bubble distribution that develops during aging.

The interpretation of the results from this study were made difficult by the complex nature of the tritium interactions with the microstructure of the base plates and the subsequent helium bubble distribution that develops during aging. This underscores the need for a thorough microstructural characterization of the starting plates prior to tritium charging as well as a comprehensive analysis of the helium distribution in each plate prior to welding. Figures 8-12 accurately depict the data generated during the course of this study; however, direct comparison of this data and validation of current results with past data is not possible without further study.

CONCLUSIONS

Metallographic examinations of weld cross-sections show that significantly more porosity exists in the 304 weld beads when compared to the 316LN welds. This result indicates that more helium was present in the 304 plate at the time of welding and that helium analyses made from test coupons did not accurately represent the helium concentration differences in the 0.5 in. plates. Thus, the seemingly reduced susceptibility to helium embrittlement cracking observed in the 316LN plate may not be an inherent quality of the material, but an effect of lower helium content when compared to the 304 plate. Possible reasons for lower helium content (reduced tritium uptake) include microstructural and alloying element differences in the plates as well as differences in surface conditions at the time of tritium charging. Therefore, a direct comparison of the underbead cracking associated with the welds on these two plates is not possible until more rigorous helium analyses are performed on the actual 0.5 in. charged-and-aged plates. This work does, however, support previous studies that have shown that low heat input overlay welding in the presence of helium is clearly more forgiving as a repair technique than stringer beads.

FUTURE PLANS

Extensive helium analyses of the two 0.5 in. thick plates examined in this study are required before a complete analysis of the helium embrittlement cracking data can be performed. Additional helium analysis would verify the distribution of helium within the plates and provide a better comparison for cracking susceptibility in the 304 and 316LN steels. An understanding of the differences in cracking and helium bubble formation during welding of the two materials could emerge from this comparison.

Additional plates that were charged and welded remain unexamined. An analysis of these plates, such as was done for the two plates discussed in this report, would accomplish the following:

- The relative weldability of the two materials would be verified for a helium content of approximately half that of the plates examined for this report.

- The effect of plate thickness on the amount of cracking would be evaluated for plates 0.030, 0.060, 0.125, and 0.5 inch in thickness. This is important to substantiate the effects of restraint caused by the wall thickness of the material and to help correlate results at ORNL on thin plate with those on thick plate at Savannah River.

- The effect of cold work on weldability would be determined. This could provide more data on how helium embrittlement takes place.

The most challenging part of the work needed to obtain these additional results has been completed. Preparation of the charged, aged, and welded samples was done along with the preparation of the samples discussed in this report. These plates are therefore a valuable source of experimental material available for further study. Additional funding is needed to complete the analysis of the remaining samples.

ACKNOWLEDGMENTS

The authors would like to express their appreciation to M. R. Louthan, Jr. for his valuable technical input, to M. J. Morgan and K. L. Shanahan for their assistance (and persistence) in providing the tritium-charged-and-aged plates, and to D. Z. Nelson and C. N. Foreman for preparing and photographing the weld cross-sections analyzed in this study.

REFERENCES

1. M. R. Louthan, Jr., W. R. Kanne, Jr., M. H. Tosten, D. T. Rankin, B. J. Cross, "Helium Embrittlement Model and Program Plan for Weldability of ITER Materials", US DOE Report WSRC-TR-97-0031, February 1997.

2. M. H. Tosten, D. Z. Nelson, W. R. Kanne, Jr., M. R. Louthan, Jr., D. T. Rankin, B. J. Cross, "A Comparison of Substructure in Welded Irradiated and Tritium Aged Stainless Steel as Observed by Transmission Electron Microscopy", US DOE Report WSRC-TR-97-00376, January 1998.

3. J. P. Maloney, "Repair of a Nuclear Reactor Vessel", Trans. Am. Nuclear Soc., Vol. 12 (supp.), 1969, pp. 38-39.

4. W. R. Kanne, Jr., "Remote Reactor Repair: GTA Weld Cracking Caused by Entrapped Helium", Welding Journal, Vol. 67, No. 8, August 1988, pp. 33-39.

5. E. A. Franco-Ferreira and W. R. Kanne, Jr., "Remote Reactor Repair: Avoidance of Helium-Induced Cracking Using GMA Welding", Welding Journal, Vol. 71, No. 2, February 1992, pp. 43-51.

6. W. R. Kanne, Jr., G. T. Chandler, D. Z. Nelson, E. A. Franco-Ferreira, "Welding Irradiated Stainless Steel", J. Nuc. Mater., Vol. 225, August (II) 1995, pp. 69-75.

7. C. A. Wang, M. L. Grossbeck, H. Aglan, and B. A. Chin, "The Effect of an Applied Stress on the Welding of Irradiated Steels", J. Nuc. Mater., Vol. 239, 1996, p. 85.

8. C. A. Wang, M. L. Grossbeck, B. A. Chin, "Threshold Helium Concentration to Initiate Cracking During Welding of Irradiated Stainless Steel", J. Nuc. Mater., Vol. 225, August (II) 1995, pp. 59-68.

9. K. Nakata, H. Takeda, and M. Oishi, "Development of Repair-Welding Technology for Irradiated Materials of LWR" The 9th International Conference on Environmental Degradation of Materials in Nuclear Power Systems – Water Reactors, August 3, 1999.

10. K. Watanabe, S. Jitsukawa, S. Hamada, T. Kodaira, and A. Hishinuma, "Weldability of Neutron-Irradiated Type 316 Stainless Steel", Fusion Engineering and Design, Vol. 31, 1996, pp. 9-15.

11. M. R. Louthan, Jr., J. A. Donovan, and G. R. Caskey, Jr., "Tritium Absorption on TYPE 304L Stainless Steel", Nucl. Technol., Vol. 26, June 1975, pp. 192-200.

12. G. R. Caskey, Jr. and R. D. Sisson, Jr., "Hydrogen Solubility in Austenitic Stainless Steels", Scripta Met., Vol. 15, 1981, pp. 1187-90.

13. S. Ningshen, M. Uhlemann, F. Schneider, and H. S. Khatak, "Diffusion Behavior of Hydrogen in Nitrogen Containing Austenitic Alloys", Corros. Sci., Vol. 43, 3001, pp. 2255-64.
14. M. J. Morgan and M. H. Tosten, "Tritium and Decay Helium Effects on the Fracture Toughness Properties of Types 316L, 304L, and 21Cr-6Ni-9Mn Stainless Steels", Proceedings of the Fifth International Conference on the Effects of Hydrogen on the Behavior of Materials, A. W. Thompson and N. R. Moody, eds., TMS, Warrendale, PA, 1996, pp. 873-82.

15. M. H. Tosten and P. A. Kestin, "Helium Bubble Distributions Beneath GMA Weld Overlays in Type 304 Stainless Steel", Microstructural Science, Vol. 19, August 1992, p. 3-12.

16. W. R. Kanne, Jr., D. A. Lohmeier, K. A. Dunn, and M. H. Tosten, "Metallographic Analysis of Helium Embrittlement Cracking of Repair Welds in Nuclear Reactor Tanks", Mater. Char., Vol. 30, 1993, pp. 23-34.

Table 1
Alloy Composition (wt.%)

Type 304		Type 316LN-IG*	
C	0.073	C, min-max	0.015-0.03
Mn	1.390	Mn, min-max	1.60-2.00
P	0.023	P, min-max	0.025 max
S	0.016	S, min-max	0.005-0.010
Si	0.520	Si, min-max	0.50 max
Ni	8.280	Ni, min-max	12.0-12.5
Cr	18.22	Cr, min-max	17.0-18.0
N	0.026	Mo, min-max	2.30-2.70
Fe	Bal.	N, min-max	0.06-0.08
		Nb+Ta+Ti, min-max	0.15 max
		Cu, min-max	0.30 max
		Co, min-max	0.25 max
		B, ppm	20 max
		Fe	Bal.

* Composition of 316LN plate within listed ranges

Table 2
Tritium-Charging Schedule

Alloy	Plate Thickness (in.)	Charging Run
304	0.5	1
316LN	0.5	1
316LN	0.125	1
316LN	0.060	1
316LN	0.030	1
304	0.5	2
316LN	0.5	2
316LN	0.125	2
316LN-CW*	0.125	2

* 50% cold-worked

Table 3
Welding Conditions

Run #1

Alloy	He (appm)	Plate Thick-ness (in)	Weld Type O/S*	Filler Wire	Oscillation Speed S_0 (in/min)	Travel Speed S_T (in/min)	I (amps)	E (volts
304	85.6	0.5	O	308L	80	3.25	75	19
			S	None	N/A	25	100	18.3
			S	None	N/A	18	100	18.6
			S	None	N/A	6	101	18.4
			S	None	N/A	3.25	100	18.5
			S	None	N/A	18	31	20
316LN-A$^+$	91.3	0.5	O	316L	80	3.25	69	19
316LN-B			O	316L	80	3.25	72	19
			S	None	N/A	25	100	19.4
			S	None	N/A	18	100	18
			S	None	N/A	6	100	17.8
			S	None	N/A	3.25	100	18.2
			S	None	N/A	18	32	21
316LN	91.3	0.125	O	316L	80	3.25	74	19
			S	None	N/A	25	41	19
			S	None	N/A	18	41	20
			S	None	N/A	6	41	19.5
			S	None	N/A	3.25	41	18
			S	None	N/A	18	32	21
316LN	91.3	0.060	O	316L	80	3.25	41	18
			S	None	N/A	6	30	19
			S	None	N/A	3.25	30	18
			S	None	N/A	18	32	20.4
316LN	91.3	0.030	S	None	N/A	32	32	18
			S	None	N/A	25	32	19
			S	None	N/A	18	32	18

Table 3 - Continued

Run #2

304	68.1	0.5	O	308L	80	3.25	72	19
			S	None	N/A	25	100	19.3
			S	None	N/A	18	100	18.6
			S	None	N/A	6	100	18.2
			S	None	N/A	3.25	100	18
			S	None	N/A	18	32	21
316LN-A	65.7	0.5	O	316L	80	3.25	72	19
316LN-B			O	308L	80	3.25	72	19
			S	None	N/A	25	100	19
			S	None	N/A	18	100	19
			S	None	N/A	6	100	18.6
			S	None	N/A	3.25	100	18.3
			S	None	N/A	18	33	18
316LN	65.7	0.125	O	316L	80	3.25	72	19
			S	None	N/A	25	40	19
			S	None	N/A	18	40	20
			S	None	N/A	6	40	19.5
			S	None	N/A	3.25	40	19
			S	None	N/A	18	32	21
316LN-CW‡	65.7	0.125	O	316L	80	3.25	73	19
			S	None	N/A	25	41	20
			S	None	N/A	18	41	19
			S	None	N/A	6	41	18.5
			S	None	N/A	3.25	41	19
			S	None	N/A	18	32	21

---

* O - GMA overlay weld, S - GTA stringer bead

\+ A - side of plate with stringer beads, B - underside of plate

‡ 50% cold-worked

Table 4
Crack Analysis Summary

GMA Overlay Welds

Plate Type*	I (amps)	E (volts)	Travel Speed (in/min)	Heat Input (kJ/in^2)	He Conc. (appm)	Number Cracks/ Weld Length (#/in)	Total Crack Length/ Weld Length (in/in)
304	72	19	3.25	23.4	85.6	23.8	0.33
Control						0.0	0.0
316LN-A**	69	19	3.25	21.5	91.3	1.9	0.01
Control						0.0	0.0
316LN-B**	72	19	3.25	22.4	91.3	0.0	0.0
Control						0.0	0.0

* ½ in. thick plate, constrained during welding, Control: 0 appm He, run-on tab
** A & B signify top (same side as GTA welds) and bottom of plate, respectively.

Table 5
Crack Analysis Summary

GTA Stringer Beads

Plate Type*	I (amps)	E (volts)	Travel Speed (in/min)	Heat Input (kJ/in^2)	He Conc. (appm)	Number Cracks/ Weld Length (#/in)	Total Crack Length/ Weld Length (in/in)
304	100	18.3	25	28.7	85.6	70.9	0.77
	100	18.6	18	38.8	85.6	31.8	0.46
	101	18.4	6	84.5	85.6	46.2	0.60
	100	18.5	3.25	136.6	85.6	26.7	0.70
	31	20	18	26.5	85.6	83.7	0.57
316 LN	100	19.4	25	28.2	91.3	19.0	0.12
	100	18	18	35.3	91.3	34.0	0.27
	100	17.8	6	91.3	91.3	16.7	0.18
	100	18.2	3.25	137.1	91.3	10.8	0.14
	32	21	18	28.8	91.3	20.5	0.11

* ½ in. thick plate, constrained during welding

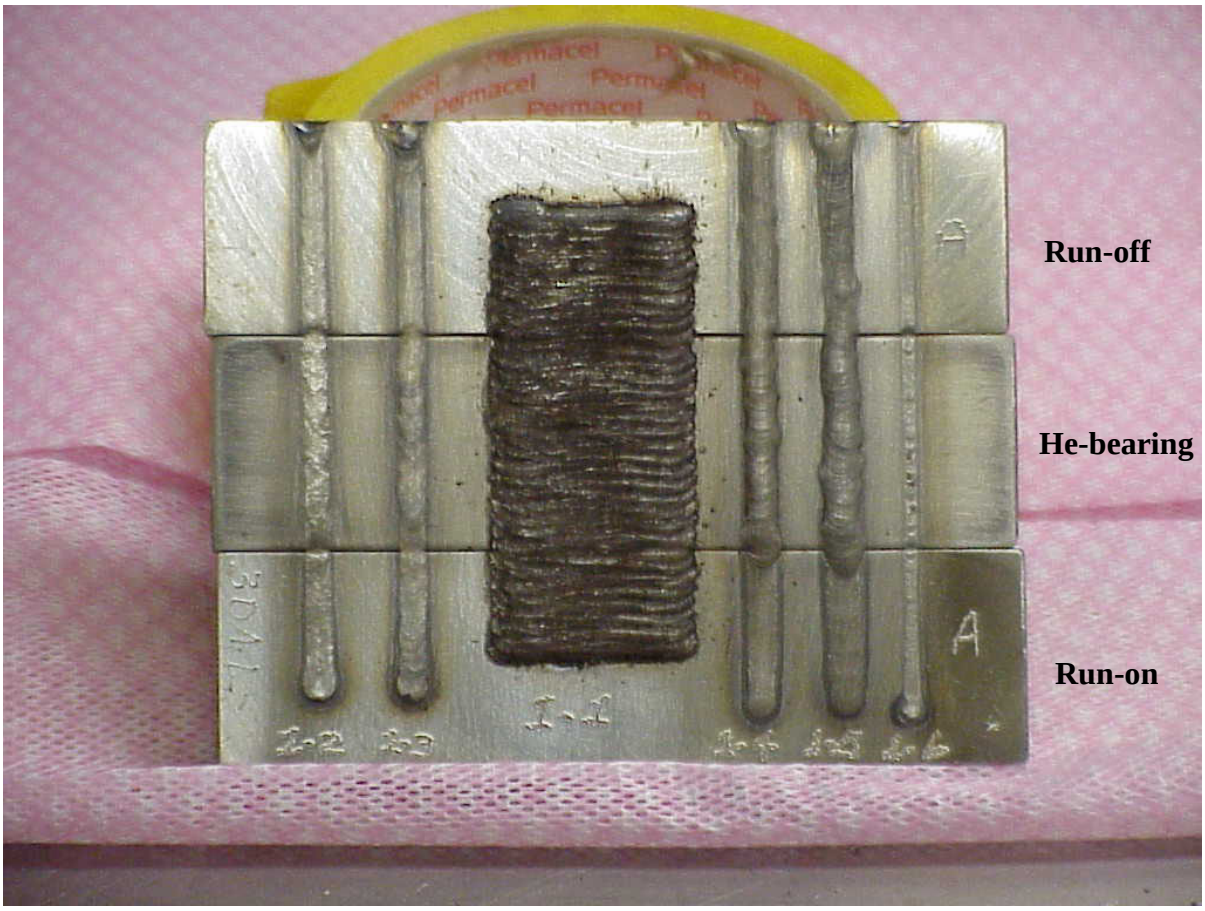

Figure 1. Typical Weld/Plate Configuration. GMA overlay in center with stringer beads. Lower plate is run-on tab (start of welds), middle plate contains tritium/helium, and the upper plate is run-off tab (end of welds).

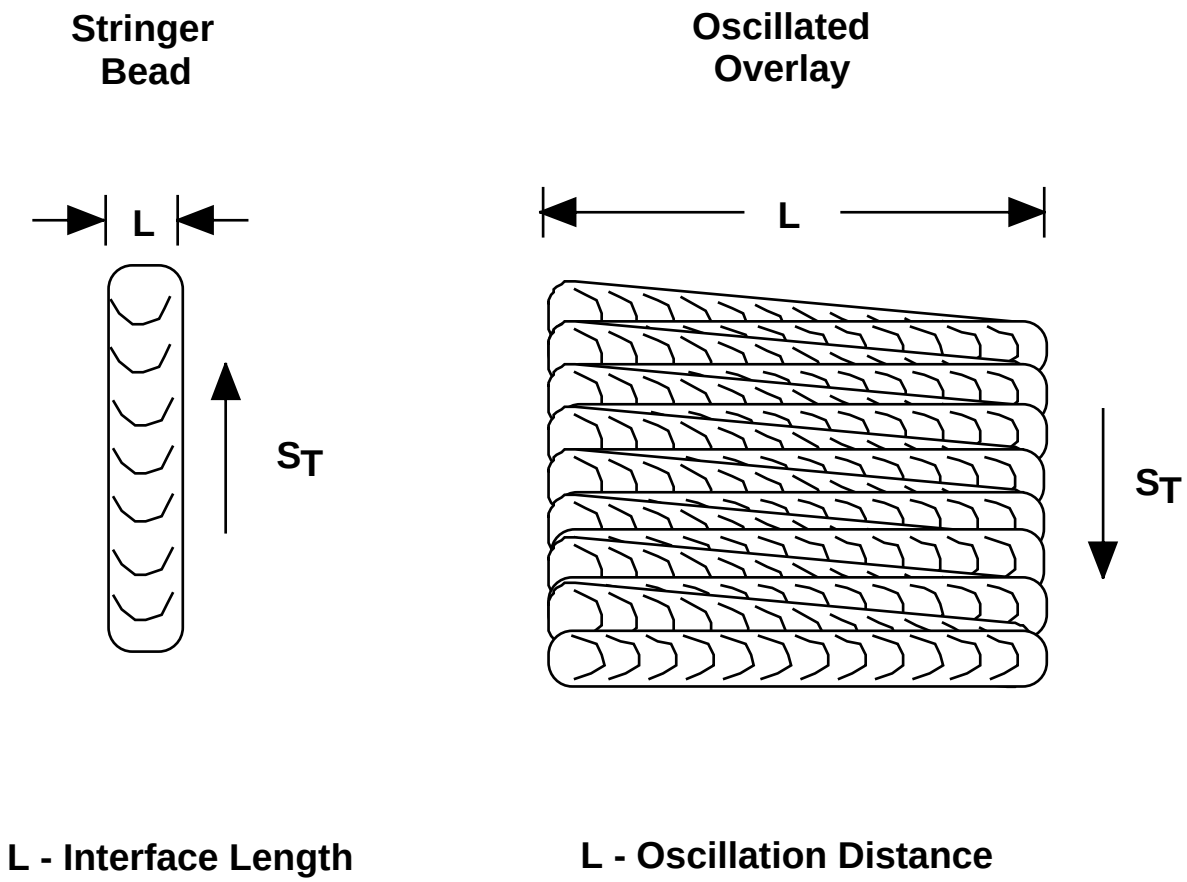

$$\text{Heat Input (kJ/in}^2) = \frac{V\,A}{L\,S_T}$$

Figure 2. Schematic diagram illustrating the heat input calculations for GTA stringer beads and GMA overlays.

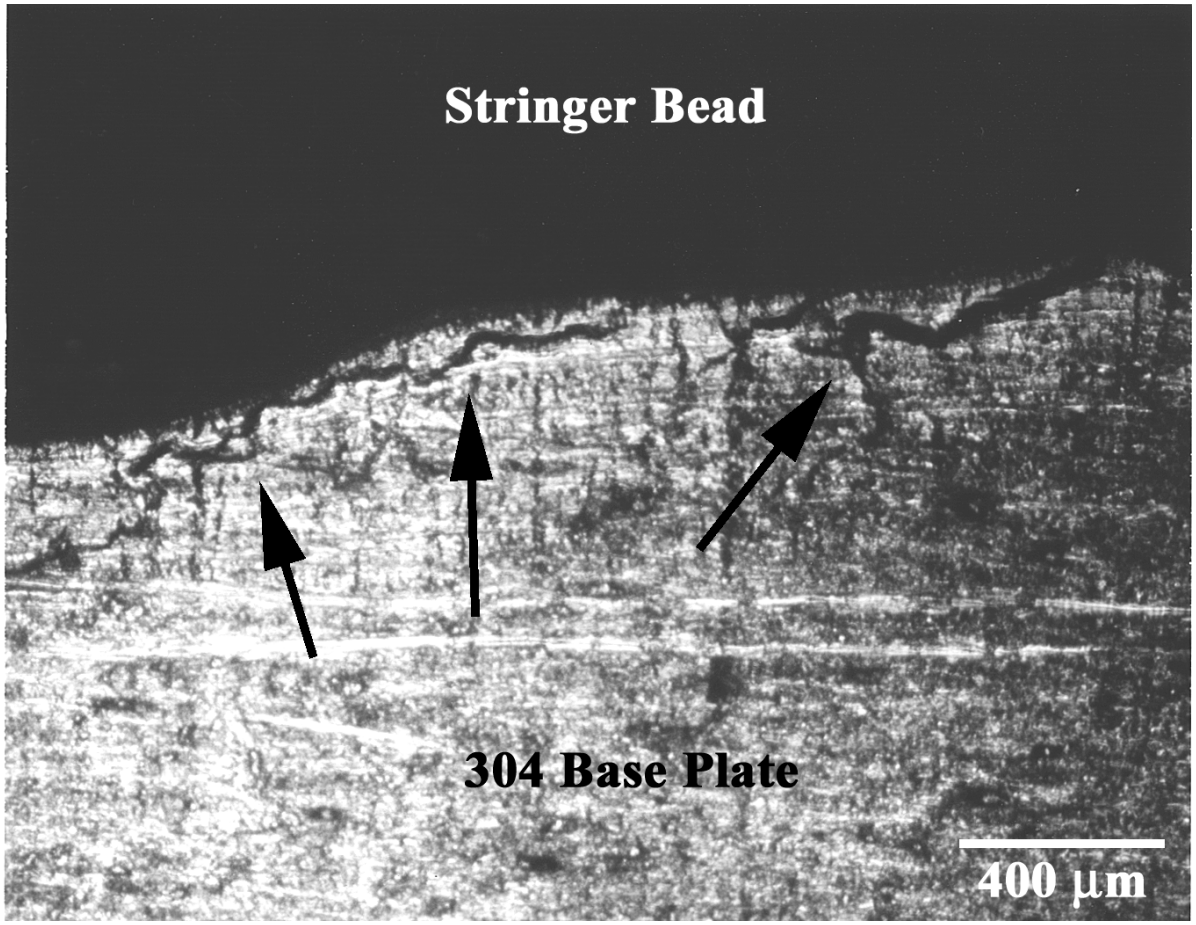

Figure 3. Toe cracking in HAZ of "hottest" stringer bead on 304 base plate.

Figure 4. GMA Overlay on 304 base plate. Helium embrittlement cracking is visible in base metal. Some cracking extends into the weld metal.

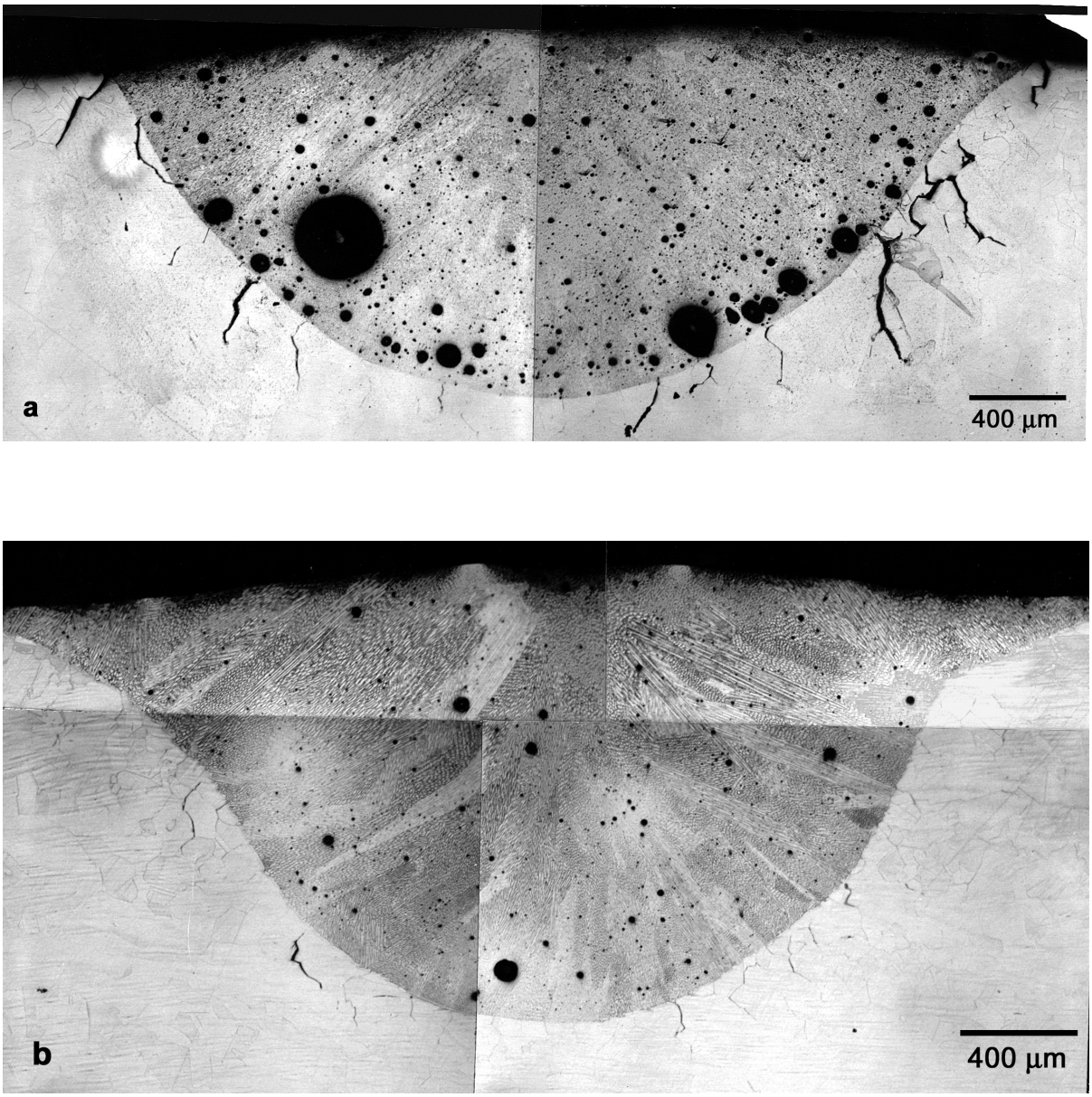

Figure 5. Cross-section of stringer beads in the a) 304 and b) 316LN plates. These welds were made using the same parameters. Notice the increased cracking and porosity in the 304 weld.

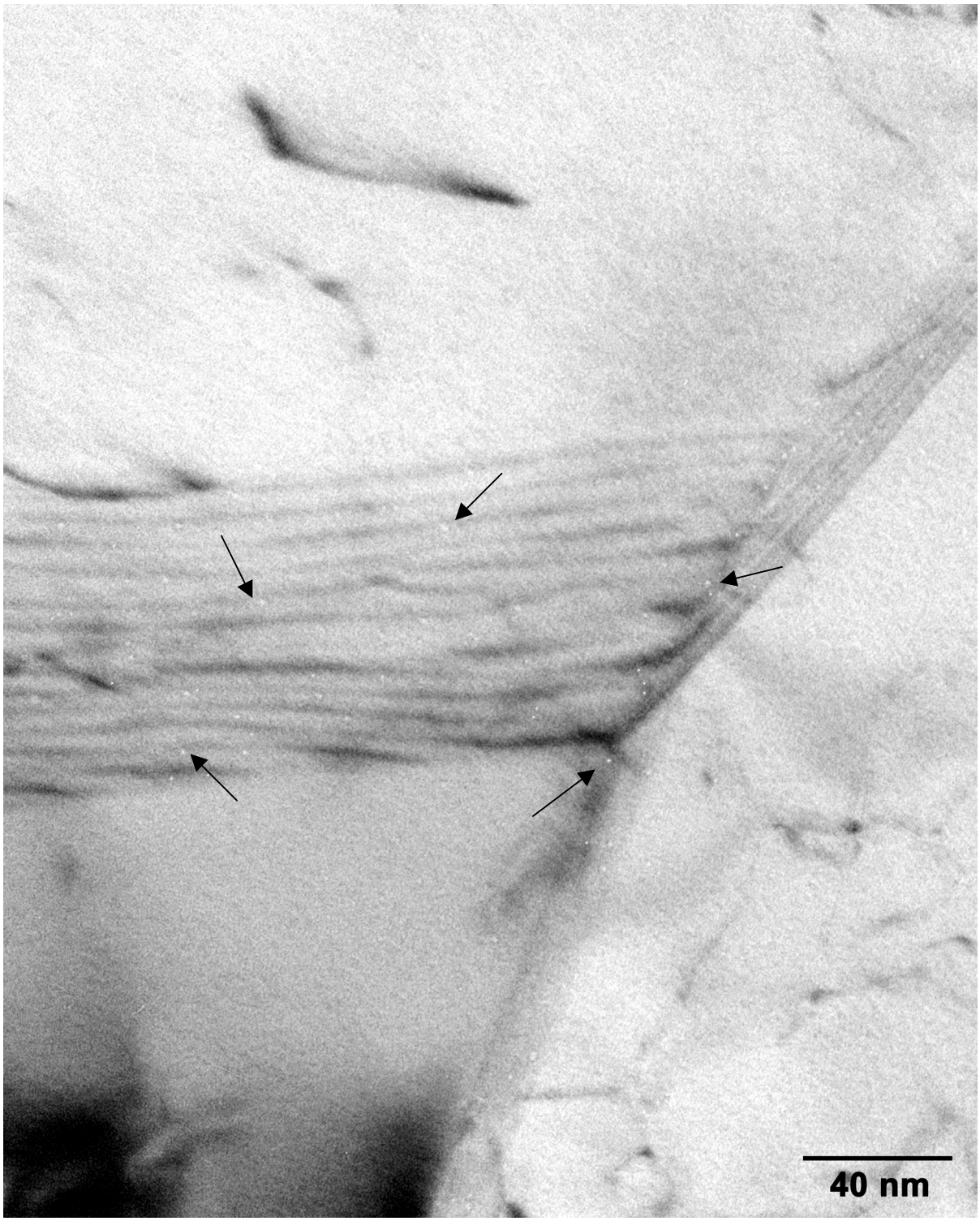

Figure 6. TEM image showing numerous small (<3 nm dia.) helium bubbles (e.g., white dots at arrows) on grain boundaries at a triple junction in 316LN - about 0.050 in. (1.27 mm) below the weld overlay.

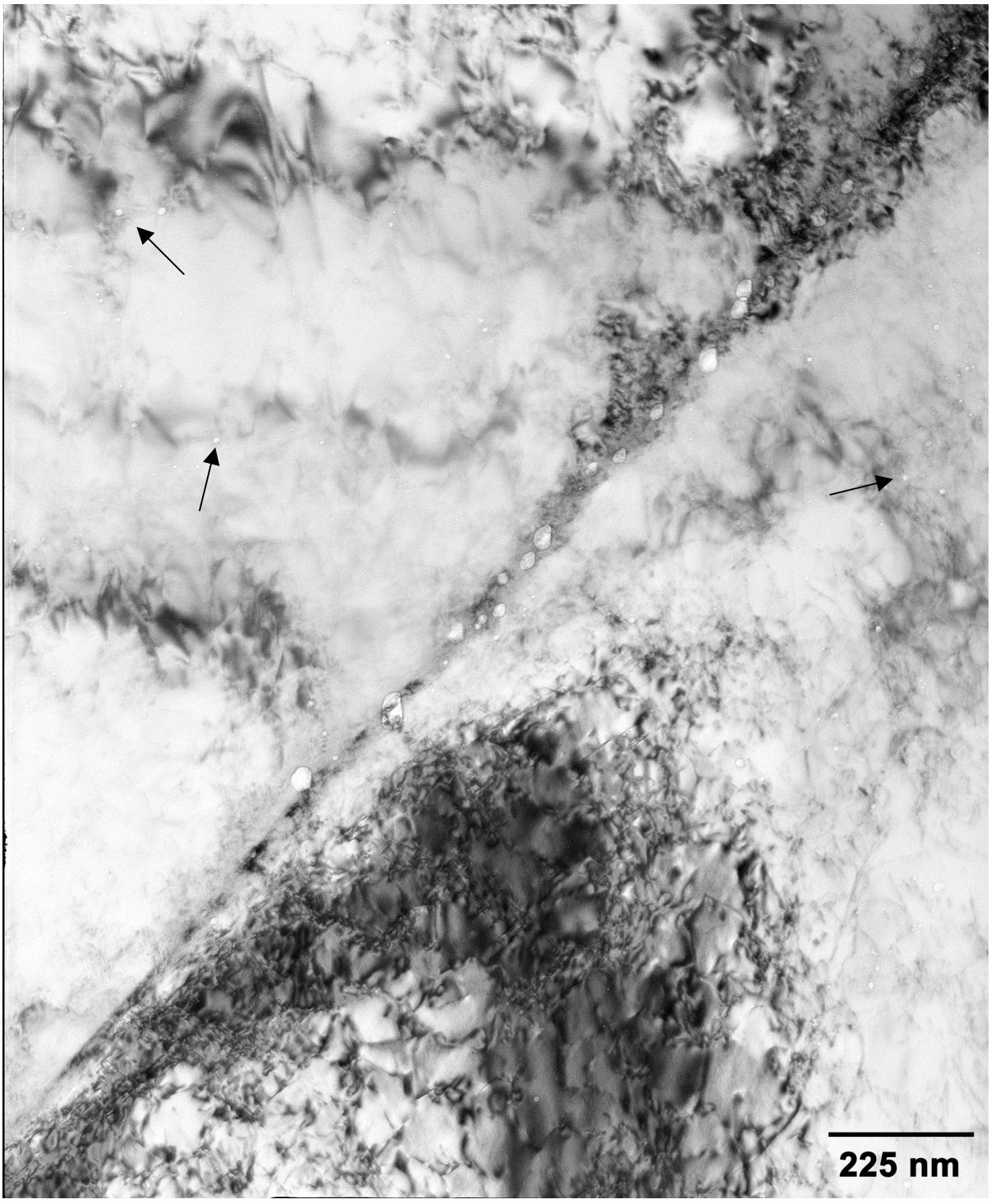

Figure 7. TEM image of large (up to 50 nm dia.) bubbles on a grain boundary and within the austenite matrix (e.g., at arrows) at about 0.010 in. (0.25 mm) below the overlay interface in 316LN.

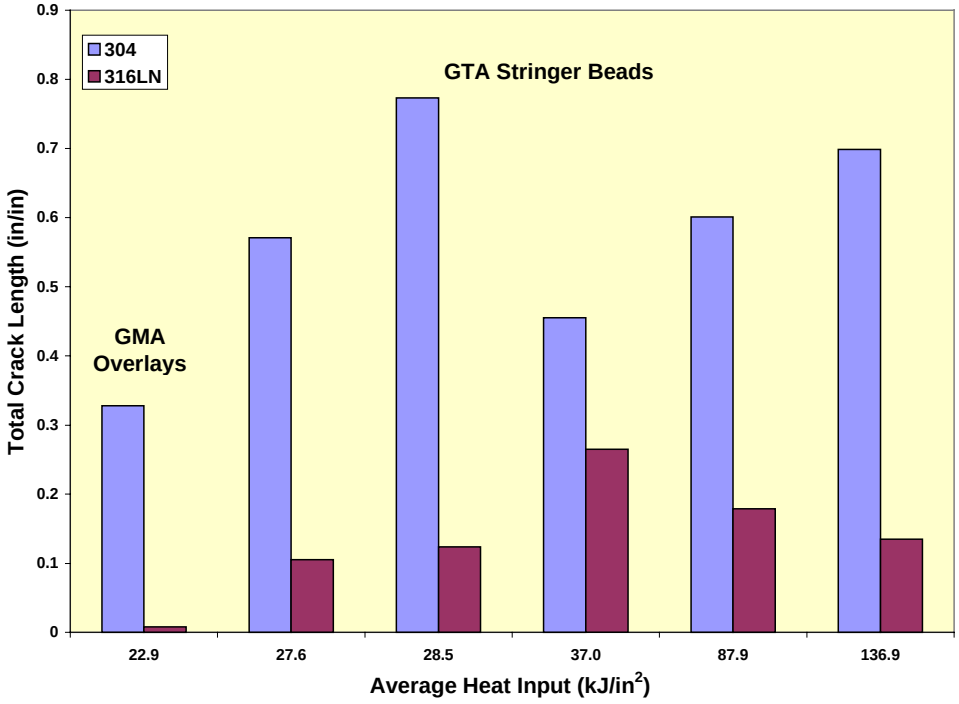

Figure 8. Total crack length for overlays (at 22.9 kJ/in^2) and stringer beads at each heat input (average of the 304 and 316LN weld values). Differences in cracking behavior may be a result of He concentration variations and/or weldability.

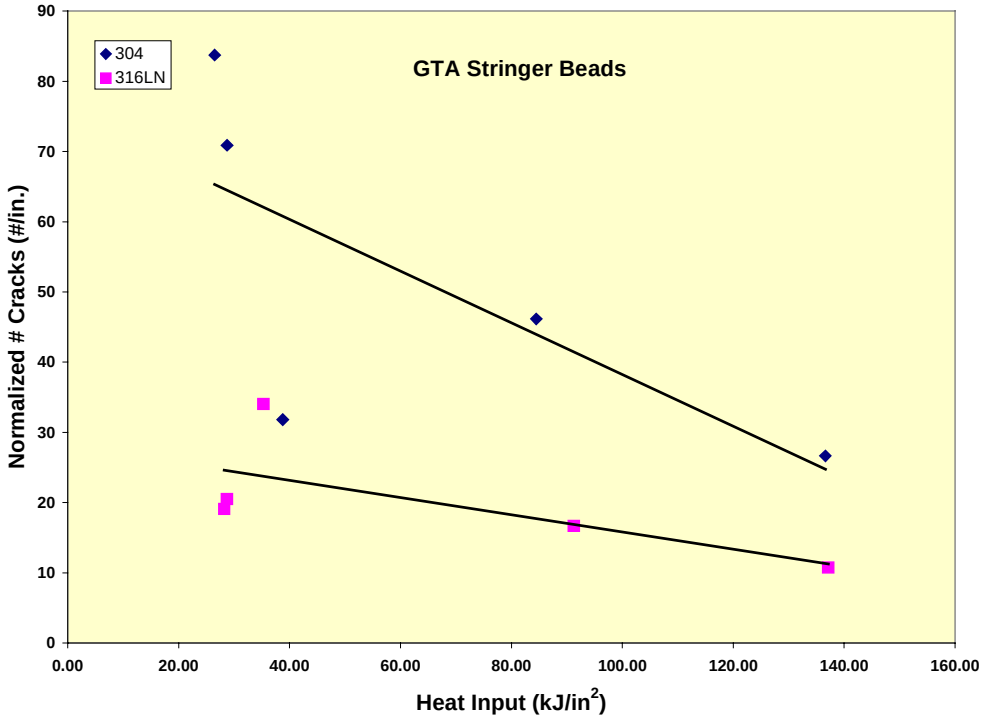

Figure 9. Total number of cracks per unit length of weld interface for the stringer beads assuming similar He contents in both steels.

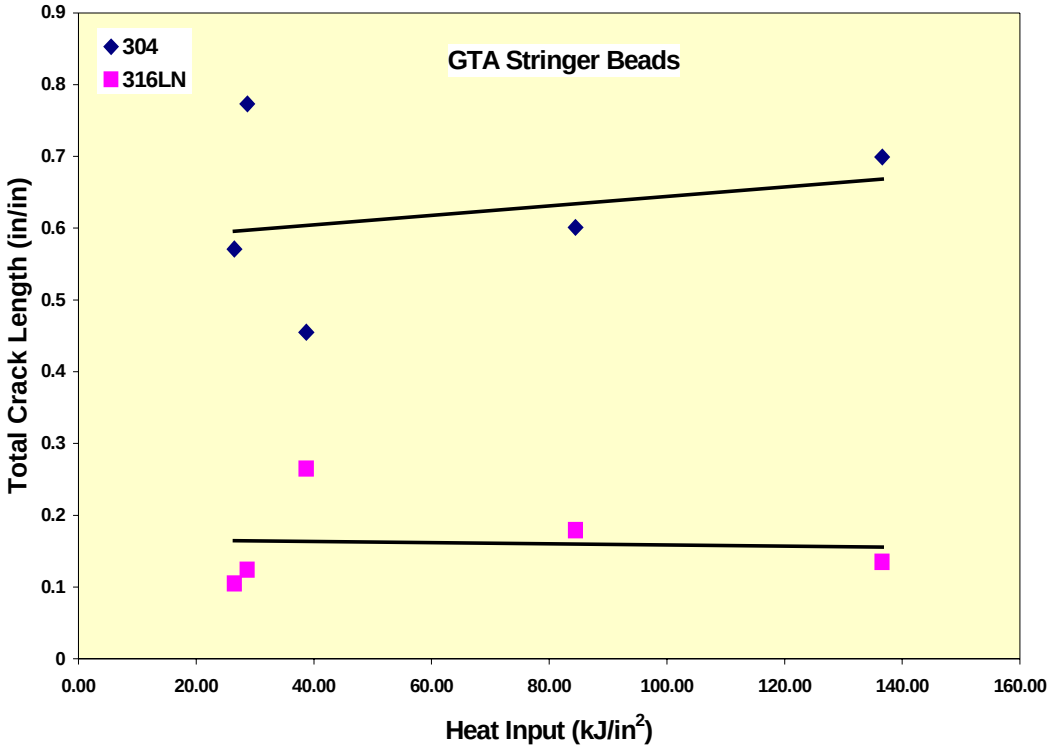

Figure 10. Total crack length vs. weld heat input for the stringer beads. Increased cracking in the 304 may be due to higher helium levels.

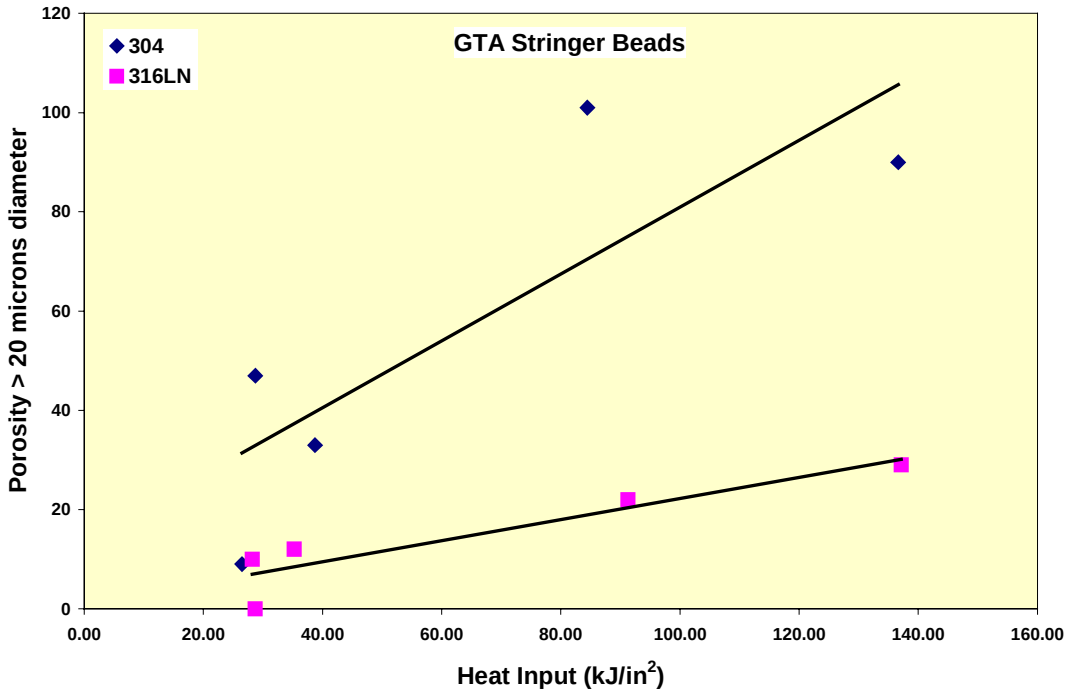

Figure 11. Porosity in stringer beads vs. weld heat input. More porosity in the 304 welds may indicate a higher helium content than in the 316LN plate.

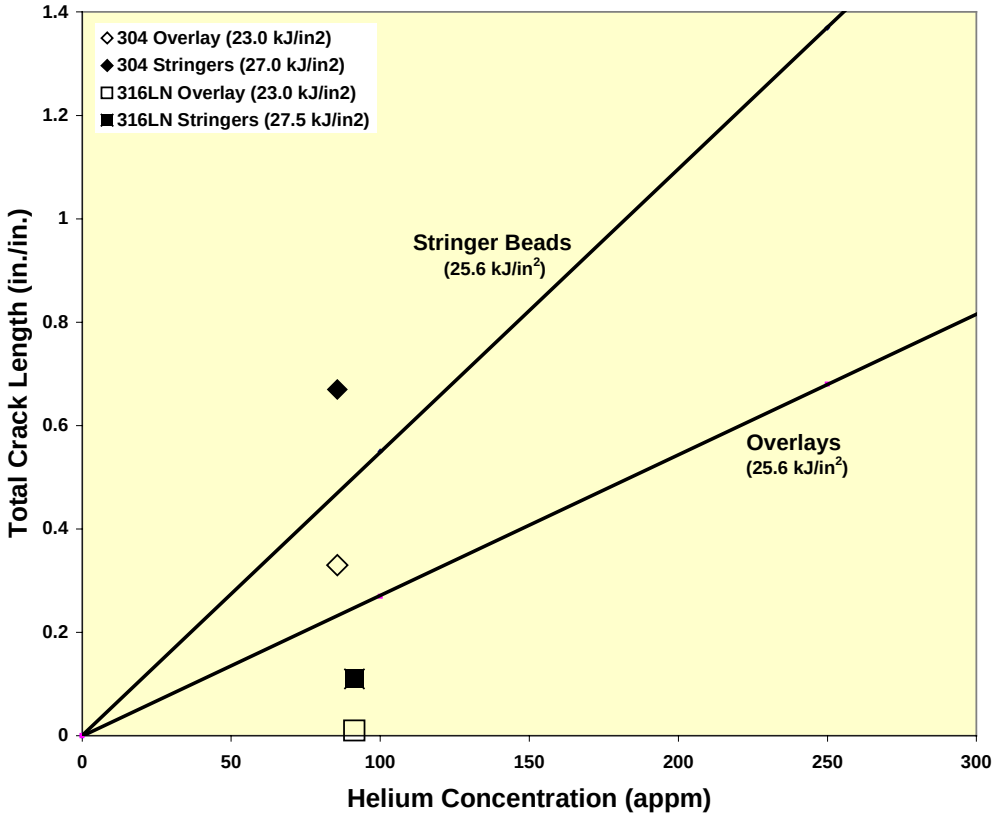

Figure 12. Crack length data plotted as a function of base metal helium concentration. The four individual data points are from the current study. The data from a previous study [Ref. 5] at SRTC of overlay welds and stringer beads on tritium-charged-and-aged 304 plates are plotted as straight lines.